Journal of Alloys and Compounds 510 (2012) 134–140

Contents lists available at SciVerse ScienceDirect

Journal of Alloys and Compounds

journal homepage: www.elsevier.com/locate/jallcom

Electrical and thermal characterization of Sm^{3+} doped ceria electrolytes synthesized by combustion technique

R.V. Mangalaraja[a,*], S. Ananthakumar[b], M. Paulraj[c], H. Pesenti[a], Marta López[a], Carlos P. Camurri[a], Loreto A. Barcos[d], Ricardo E. Avila[d]

[a] Department of Materials Engineering, University of Concepción, Concepción, Chile
[b] Materials and Minerals Division, National Institute for Interdisciplinary Science and Technology (NIIST), CSIR, Trivandrum, India
[c] Department of Physics, University of Concepción, Chile
[d] Department of Nuclear Materials, Chilean Nuclear Energy Commission, Santiago, Chile

ARTICLE INFO

Article history:
Received 25 October 2010
Received in revised form 20 May 2011
Accepted 4 September 2011
Available online 10 September 2011

Keywords:
Doped ceria
Ceria nanoparticles
Samarium
Combustion synthesis
Electrical conductivity
Thermal property

ABSTRACT

Nanocrystalline samarium doped ceria electrolyte [$Ce_{0.9}Sm_{0.1}O_{1.95}$] was synthesized by citrate gel combustion technique involving mixtures of cerium nitrate oxidizer (O) and citric acid fuel (F) taken in the ratio of $O/F = 1$. The as-combusted precursors were calcined at 700 °C/2 h to obtain fully crystalline ceria nano particles. It was further made into cylindrical pellets by compaction and sintered at 1200 °C with different soaking periods of 2, 4 and 6 h. The sintered ceria was characterized for the microstructures, electrical conductivity, thermal conductivity and thermal diffusivity properties. In addition, the combustion derived ceria powder was also analysed for the crystallinity, BET surface area, particle size and powder morphology. Sintered ceria samples attained nearly 98% of the theoretical density at 1200 °C/6 h. The sintered microstructures exhibit dense ceria grains of size less than 500 nm. The electrical conductivity measurements showed the conductivity value of the order of 10^{-2} S cm^{-1} at 600 °C with activation energy of 0.84 eV between the temperatures 100 and 650 °C for ceria samples sintered at 1200 °C for 6 h. The room temperature thermal diffusivity and thermal conductivity values were determined as 0.5×10^{-6} m^2 s^{-1} and 1.2 W m^{-1} K^{-1}, respectively.

1. Introduction

Synthesis of rare earth doped ceria is a subject of interest because of its potential application as electrolyte for the low temperature solid oxide fuel cells (LT-SOFCs). Depending upon the dopant's nature, ceria can be tuned as either oxygen ionic-conductors or ionic–electronic mixed conductors. For enhancing the ionic conductivity of ceria electrolytes dopants having ionic radii close to ceria are usually preferred [1]. Doping of R^{3+} ions (R = rare earths, like Sm, Gd, Nd, Y, Pr, etc.,) in the crystal structure of ceria enhance the bulk ionic conductivity of ceria by increasing the extrinsic oxygen vacancy density due to reduction of Ce^{4+} to Ce^{3+} [1,2]. CeO_2 prepared with these dopants are claimed to have low redox stability than the conventional yttria stabilised zirconia (YSZ). They begin to show significant electronic conductivity because of the variable oxidation states of Ce at higher temperatures, especially under reducing conditions. The ionic conductivity of an electrolyte strongly depends on the concentration, formal charge and ionic radius of the dopant cations. The earlier research works have successfully demonstrated that the partial substitutions by di- or trivalent cations generate oxygen vacancies and maintain the charge neutrality of the CeO_2 crystal lattice. The doping has introduced enhanced conductivity primarily caused by the oxygen vacancies.

Among various rare earth trivalent dopant ions (Gd^{3+}, Sm^{3+}, Y^{3+}, Nd^{3+} and La^{3+}), Sm^{3+} has been found to yield high oxygen–ion conductivity at certain fixed doping levels. One of the reasons is, it has the smallest association enthalpy between the dopant cations and oxygen vacancies in the fluorite lattice [3]. Sm^{3+} doping introduces oxygen vacancies into CeO_2 lattice as per the following defect reaction:

$$Sm_2O_3 \rightarrow 2Sm'_{ce} + V_o^{\bullet\bullet} + 3O_o^x$$

where the symbols have their usual meanings in the Kroger–Vink notations. In this reaction each pair of Sm^{3+} cations creates one $V_o^{\bullet\bullet}$ for charge compensation. The Sm'_{ce} and $V_o^{\bullet\bullet}$ point defects tend to cluster due to static electrical attraction, and the tendency increases at higher doping levels, finally leading to the formation of larger

* Corresponding author at: Department of Materials Engineering, Faculty of Engineering, University of Concepción, 270, Edmundo Larenas, Concepción, Chile. Tel.: +56 41 2207389; fax: +56 41 2203391.
E-mail addresses: mangal@udec.cl, rvmangalaraja@hotmail.com (R.V. Mangalaraja).

0925-8388/$ – see front matter © 2011 Elsevier B.V. All rights reserved.
doi:10.1016/j.jallcom.2011.09.016

(Sm'_{Ce}–$V_o^{\bullet\bullet}$) pairs of defect aggregation [4]. In most of research, Gd and Sm doping had been seriously considered and they were found to be truly promising for LT-SOFC. Here we review some of the micro-parameters that are shown much influence on the electrical conductivities of Sm-doped CeO_2. A work reported by Kosinski et al. claimed the conductivity level of 1.81×10^{-2} S cm^{-1} at 600 °C when ceria was doped with 20% samarium [5]. This work stressed that chemical compositional homogeneities of the bulk ceria as well as the doped grain boundaries of sintered CeO_2 are critically important for enhanced electrical conductivities. In some studies, use of more than one dopant has been suggested for high electrical conductivities of ceria electrolytes. However in the case of multiple dopant, the chemical in-homogeneity was found to strongly affect the bulk conductivity. For example nanocrystalline fluorite structure ceria co-doped with Sm and Nd and sintered at 1400 °C had shown electrical conductivity only 0.012 S cm^{-1} at 500 °C [6]. Many reports have confirmed that the selection of processing techniques is infact a serious concern for having high homogeneity and enhanced electrical conductivity. For instance the sol gel derived Sm doped nano ceria had showed electrical conductivity as 0.005 S cm^{-1} which is comparatively less than the ceria processed through fuel assisted gel decomposition route [7]. Research studies also report that the conductivity increases when grain size approaches nano regime. This attracted fabricated of thin film electrolytes using meso porous, nano ceria obtained through mechano-chemical route. In this case nano structured interfaces improved the electrical conductivity. Other than chemical processing and homogeneity the extent of oxygen vacancies with respect to different dopants have also been systematically examined in a study reported by Anderson et al. which had conclusively said that the dopants should be carefully selected in a way that the atomic number varies between 61 and 62 [8]. As a new trend on composite electrolytes have been introduced which appear to be potential for the enhanced electrical conductivity and efficient cell performance.

In the topic of ceria electrolyte, scope for further research still exists in the areas of (i) chemical or physical synthesis of nano scale Sm^{3+} doped ceria for producing sinter-active bulk powders, (ii) complete densification at low sintering temperatures, (iii) fabrication of economically viable SOFC for domestic applications, and (iv) recycling of electrolyte materials. Application of combustion synthesis for ceria has advantages compared to many other chemical routes because it is simple, possibilities of scaling up by spray-combustion, efficiency for obtaining reactive ceria powders that can give low temperature densification and minimum grain-growth.

In the present study, we have synthesized Sm^{3+} doped ceria ($Ce_{0.9}Gd_{0.1}O_{1.95}$) by citrate gel combustion route and assessed its electrical and thermal properties in addition to the powder characteristics. The thermal conductivity and thermal diffusivity data for Sm^{3+} doped ceria is seldom reported. Unlike electrical conductivities, the thermal conductivity of the ceria has not been seriously taken up for evaluating the electrolytes. To the best of our knowledge, there are not many reports deal with the thermal conductivity of the Sm^{3+} doped CeO_2 electrolytes. However, few studies were devoted on thermal properties of samarium doped ceria specifically for thermal barrier coatings (TBCs) applications [9]. Concerning LT-SOFCs, the dependence of thermal conductivity with respect to processing, presence of single and multiple dopants at various concentrations, thermal conductivity variations upon grain boundary engineering and micro to nano grains size control, effect of composite electrolyte mixtures and thermal conductivity by phonon-scattering have been necessary to exploit the doped CeO_2 for SOFC applications. In this work the data derived on the electrical and thermal properties of Sm^{3+} doped ceria has better scope for processing more efficient ceria electrolytes that can be applied for LT-SOFC.

2. Experimental

2.1. Synthesis

Samarium doped ceria was prepared by dissolving nitrate precursors of cerium [$Ce(NO_3)_3{\cdot}6H_2O$, purity 99%] and samarium [$Sm(NO_3)_3{\cdot}6H_2O$, purity 99.9%] in distilled water. Citric acid [CH_2COOH COH COOH CH_2COOH, purity ≥99.5%] was used as fuel. The required amount of citric acid fuel was calculated using the basic principles of propellant chemistry, i.e. the ratio of oxidizing and reducing valencies should be unity [10]. In a typical experiment, for synthesizing one mole of $Ce_{0.9}Sm_{0.1}O_{1.95}$, 0.783 moles of citric acid was taken. A clear homogeneous precursor solution was first prepared in aqueous medium and then transferred into platinum crucible (100 ml). It was then subjected to combustion reaction in a preheated electric furnace maintained at 500 °C. When the mixture reaches the point of spontaneous combustion, it starts burning and within few minutes porous solid foam was obtained. It was collected and crushed for further calcination. During combustion reaction, release of dense brown fumes was observed. The release of gases like NO_2, N_2, CO_2, and H_2O were expected during the reaction. The calcination of the as-prepared porous $Ce_{0.9}Sm_{0.1}O_{1.95}$ powder was carried out at 700 °C/2 h in air atmosphere. The powders after calcinations were pressed uni-axially into cylindrical pellets and rectangular bars and then sintered at temperature of 1200 °C for 2, 4 and 6 h. The sintered density was measured by Archimedes principle.

2.2. Characterization

The as-prepared powders were characterized by thermogravimetric analysis at a constant heating rate of 10 °C/min in He atmosphere using a Netzsch-STA 409 PC/PG equipped with a mass spectrometer (Balzers MID) for identifying the evolved gases. Crystalline nature and phase purity were examined by powder X-ray diffraction technique (X'Pert Pro, Philips X-ray diffractometer) using Cu K_α radiation. Scherrer's equation was used for determining the crystallite size [11]. Bulk surface area of the as-prepared and calcined powders was measured using Brunauer–Emmett–Teller (BET) method in Micromeritics ASAP 2010 instrument after properly degassing the powder samples at 150 °C. Morphology, particle size and distribution were analysed by both scanning electron microscope (SEM-JEOL 6460 LV) and transmission electron microscope (TEM-JEOL JEM 2000 EX). TEM samples were prepared by dispersing the powder in dilute ethanol under ultrasonic agitation. A drop of this suspension was placed on a carbon coated fine-mesh copper grid. Once ethanol gets evaporated, samples were subjected for imaging under TEM.

The electrical properties of the sintered samples were tested by impedance spectroscopy (IS) using a Schlumberger SI-1260 impedance analyzer in the frequency range of 10 MHz to 10 mHz. Keithley 237 electrometer was employed for the DC electrical conductivity measurements between room temperature to 650 °C. The hysteresis and linearity of *dc I–V* measurement was observed using cyclic voltammetry in the voltage range −5 to +5 V. The temperature activation of the conductivity was tested both by impedance spectroscopy (IS) and current–temperature measurements. For *dc* current–temperature measurements, a 4 h ramp was programmed from ambient temperature to ~635 °C. Along this ramp, alternating $+V_o$ and $-V_o$ bias pulses (V_o = 500 mV), each 10 s long were applied and the current, I^+, I^-, was registered as the average of the last 3 measurements during the final 0.3 s, at the end of the respective pulse. The conductance was calculated using the expression

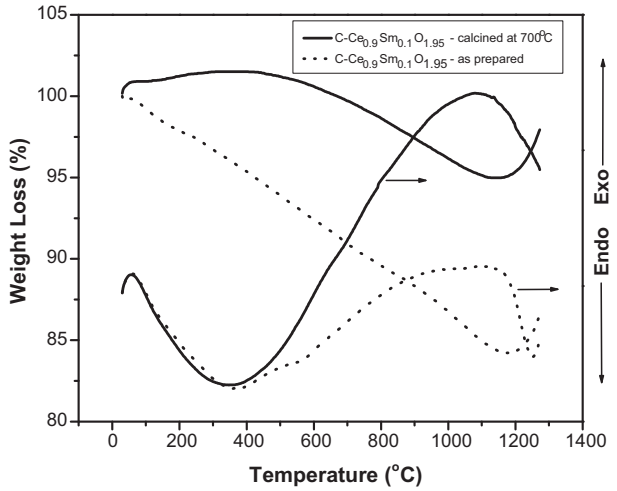

Fig. 1. Thermal analysis of as-prepared and calcined powders of $Ce_{0.9}Sm_{0.1}O_{1.95}$.

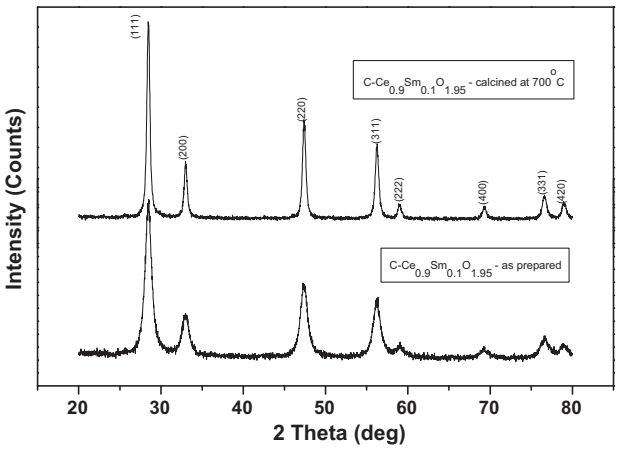

Fig. 2. X-ray diffraction pattern of the $Ce_{0.9}Sm_{0.1}O_{1.95}$ powders derived using citric acid and calcined at 700 °C.

$(I^+ - I^-)/(2V_o)$. For electrical contacts, Pt electrodes (25 nm thick, 6 mm in diameter) were applied by Ar plasma sputtering. The electroded samples were placed inside a quartz tube and heating was given by an external electrical oven. Air was circulated at 250 cm^2. The temperature was monitored by a K type thermocouple fixed within 4 mm distance from the sample surface.

The room temperature thermal diffusivity (α) values were evaluated by photoacoustic (PA) technique using a homemade PA cell. In order to determine the thermal diffusivity values, a modulated light beam from a He–Ne laser (20 mW, 632.8 nm) was irradiated on the sample placed within an enclosed PA cell. A sensitive microphone (Bruel & Kjaer, 4943 Denmark) was embedded inside the PA cell. A mechanical chopper (SR 540, Stanford Research Systems, USA) was used to modulate the excitation light beam. More details on the thermal property measurements are described elsewhere [12,13]. The room temperature thermal conductivity (λ) was calculated using the formula:

$$\lambda = \alpha \cdot \rho \cdot C_p (\mathrm{W\ m^{-1}\ K^{-1}})$$

where α is the room temperature thermal diffusivity ($m^2\ s^{-1}$), ρ is the sintered density of the sample and C_p is the specific heat capacity ($J\ kg^{-1}\ K^{-1}$). The specific heat capacity of $Ce_{0.9}Sm_{0.1}O_{1.95}$ was calculated using the heat capacity data reported in the literature for CeO_2 and Sm_2O_3. The calculation was followed as per the Neumann–Kopp rule [14]. The Neumann–Kopp rule represents the simplest approach for the estimation of mixed oxide specific heat capacity (C_{pm}) at room temperature (298.15 K). In this method, the molar heat capacity of the mixed oxide is calculated as a weighted sum of the heat capacities of the constituent oxides.

3. Results and discussion

3.1. Powder characteristics, sintering and microstructure analysis

The TG/DT analyses of the as-prepared and calcined ceria powders are presented in Fig. 1. The TG curves for both the samples showed only single-step decomposition. A comparatively faster decomposition was seen in the as-prepared samples. This cause little change in the slope of the TG curves between the samples. As expected, the calcined samples showed decreased weight loss. The total weight losses of 16 and 5 wt% were determined for the as-prepared and calcined $Ce_{0.9}Sm_{0.1}O_{1.95}$ powders, respectively. In the as prepared condition the samples contain mixture of semicrystalline and amorphous hydrated-hydroxyl species $[Ce(OH)_4{\cdot}H_2O]$ of ceria in the polymerized citrate gel network. During heating the precursor undergoes complete dehydration, dehydroxylation and possibly particle-densification as well as burning of free-carbon. These effects caused significant weight loss in the as-prepared samples. In the case of calcined samples, the weight loss occurred due to the removal of structurally bonded water and the unburnt carbon that remain even after calcination. As similar to

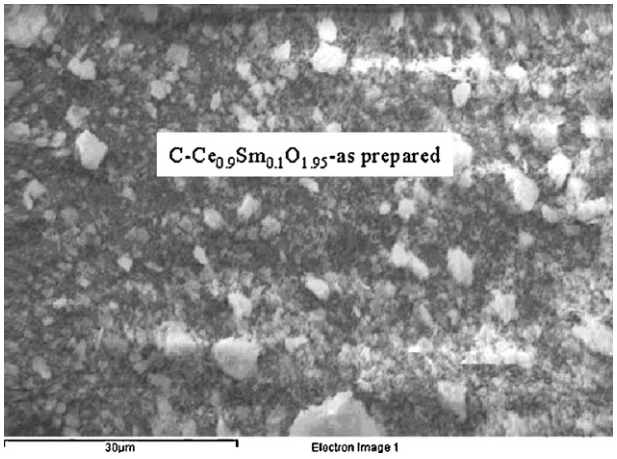

Fig. 3. SEM morphology of the as-prepared precursor foam of $Ce_{0.9}Sm_{0.1}O_{1.95}$.

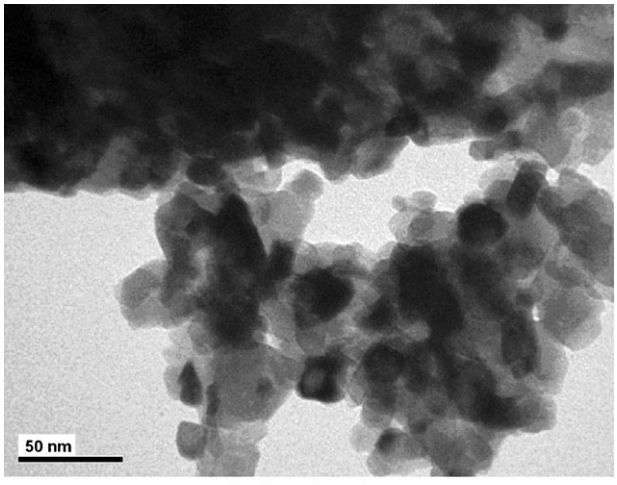

Fig. 4. TEM photographs of calcined $Ce_{0.9}Sm_{0.1}O_{1.95}$ powder.

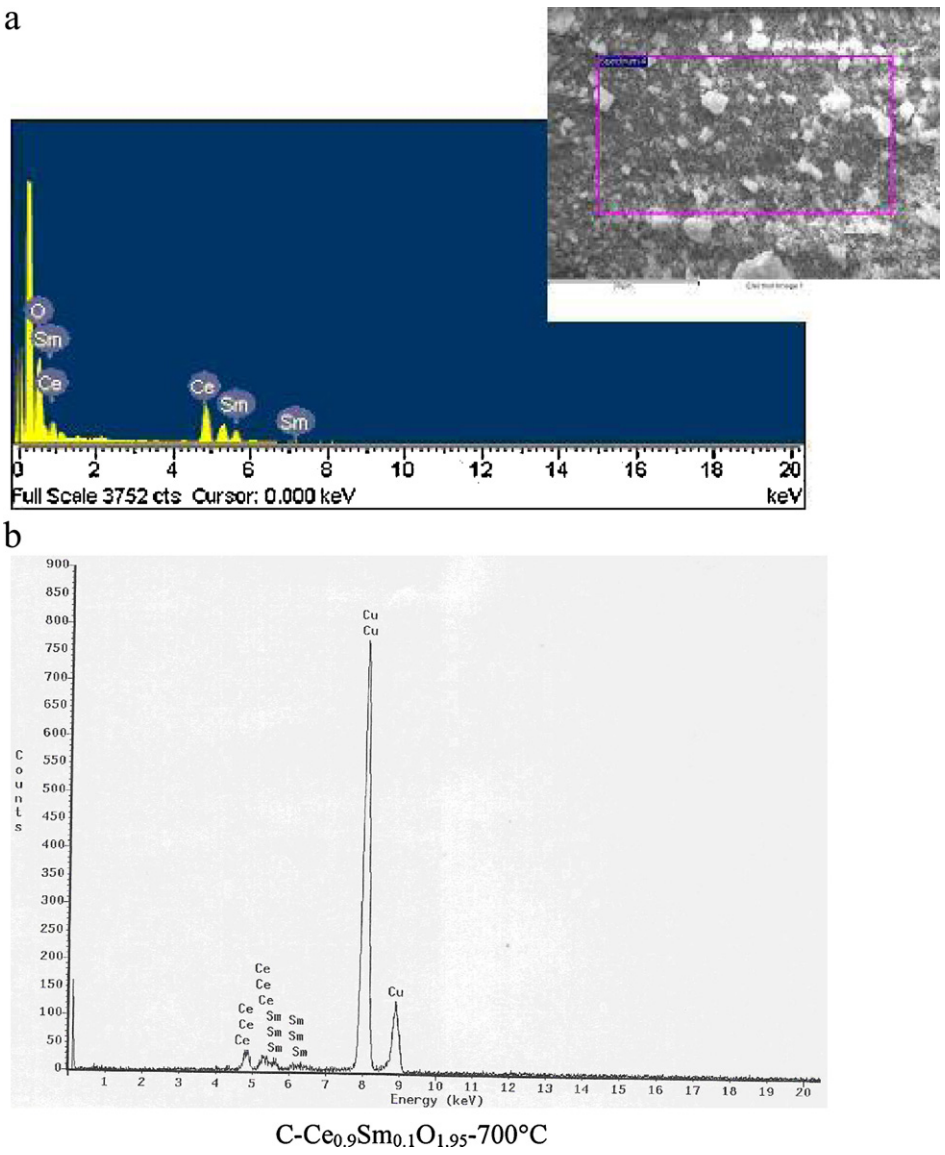

Fig. 5. Chemical analysis spectrum of EDS attached with (a) SEM and (b) TEM for calcined $Ce_{0.9}Sm_{0.1}O_{1.95}$ powder.

earlier studies, the combustion derived Sm^{3+} doped ceria also exhibits weight gain above 1000 °C. It may be associated with oxygen uptake due to Ce^{3+} oxidation into Ce^{4+}. This may occur if a part of ceria cations have 3+ oxidation states after the combustion synthesis. Such behaviour seems quite likely, especially due to the presence of carbon which reduces the ceria cations at the beginning of the reaction, i.e. initial stage of combustion. The TG curve confirmed a weight gain of 3.1% for the calcined powders at 1160 °C. The as-prepared precursor showed 2.9% weight gain between the temperatures 1190 °C to 1270 °C. Infact after calcinations at 700 °C, the $Ce_{0.9}Sm_{0.1}O_{1.95}$ powders largely contain crystalline ceria nano-clusters. At elevated temperatures the highly reactive nano ceria and its clusters will under go nucleation and growth. At temperatures nearly 1160 °C, the ceria crystals had grown to its maximum and its crystal lattice started expanding showing increased weight gain. In the as prepared precursors the presence of porous, amorphous and complex hydroxyl species of ceria agglomeration shows a strong tendency for dehydroxylation initially, and later a simultaneous crystal growth and densification. Since the densification reaction is associated with the crystal growth, the as prepared samples show marginal difference in weight gain.

The powder X-ray diffraction analysis of the as-combusted and calcined $Ce_{0.9}Sm_{0.1}O_{1.95}$ powders is shown in Fig. 2. The formation of cubic fluorite ceria is confirmed in both cases. The peaks were found to match well with the cerium oxide JCPDS card No.: 34-394. All the peaks can be assigned to the crystal planes (1 1 1) (2 0 0) (2 2 0) (3 1 1) (2 2 2) (4 0 0) (3 3 1) and (4 2 0). There are no peaks detected for the dopant samarium oxide. It indicates that the dopant ion is fully substituted in the CeO_2 lattice. Since the XRD showed fluorite type phase, we can believe that only true fluorite cubic solid-solution is formed in the system. The primary crystallite size values calculated from the X-ray broadening data were found to be 6 and 17 nm for the as-prepared and calcined powders, respectively.

The specific surface areas corresponding to the as-prepared and calcined $Ce_{0.9}Sm_{0.1}O_{1.95}$ powders are 50.8 and 36.5 m^2/g, respectively. A high surface area in the as-prepared powders is an indicative of its porous agglomerate nature and clustering of amorphous nano particles. The particle-coalescence and crystal growth during calcination significantly decreased the surface area. According to the relation $D = 6000/\rho S$ where D is the equivalent spherical diameter of the particles (in nm), ρ is the theoretical density of the material (7.179 g/cm^3) and S is the measured specific surface

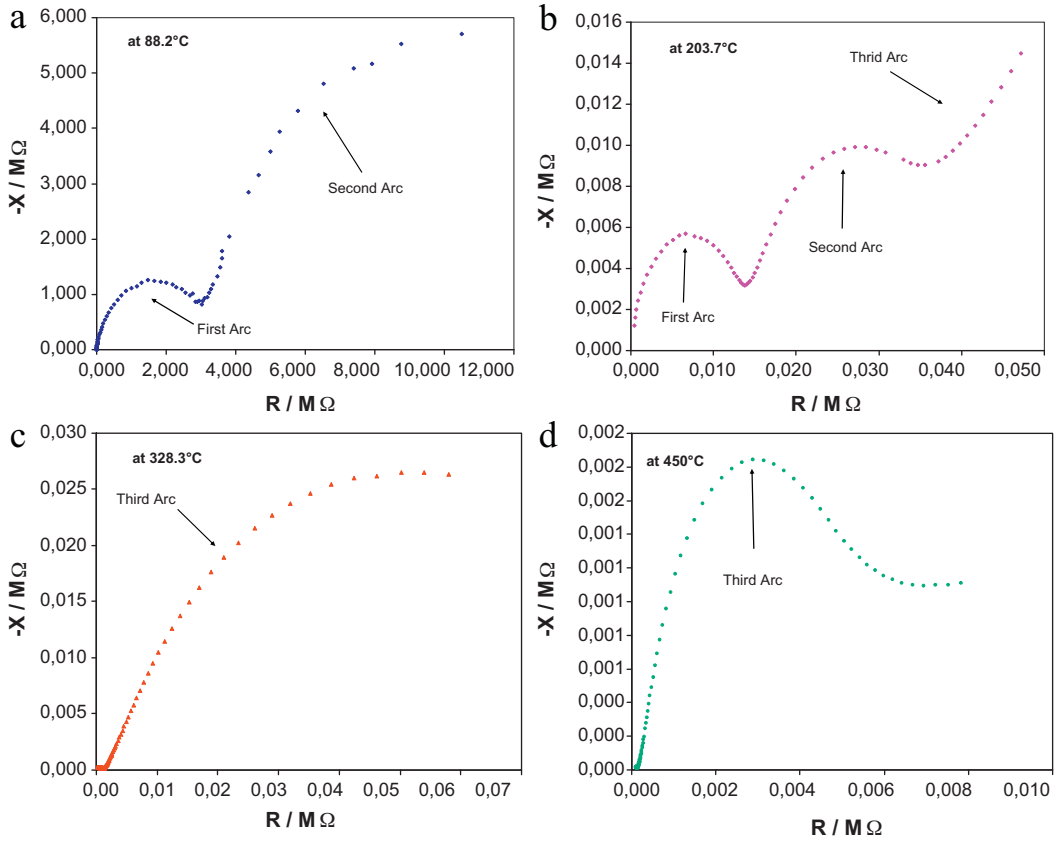

Fig. 6. Impedance plots of $Ce_{0.9}Sm_{0.1}O_{1.95}$ ceramics sintered at 1200 °C for 6 h, measured at (a) 88, (b) 203, (c) 328 and (d) 450 °C.

area (in m^2/g), the primary particle sizes of the as-prepared and calcined powders were 16.5 and 22.9 nm, respectively. It confirms that the particles have grown considerably during calcinations. This is also resulted in an overall decrease in the intra-particle pore volume. These values are at least one order higher than the particle sizes calculated from the X-ray broadening data. The particle size derived from surface area also indicates that the particles are composed of many crystallites. When the metal nitrates impregnated in the polymeric gels get ignited the evolution of gaseous products, localized heating and heat dissipation occurs within the polymeric metal nitrate–citrate gel network. The strong viscous and adhesive force in the gel network increased the inter-particle sticking to form nano-clusters, loosely packed or agglomerated particles. During calcination the individual primary crystallites or nano-clusters grow into larger grains.

The particle size and powder morphology as observed by the SEM and TEM are shown in Figs. 3 and 4. The as-prepared powders show spongy, thin flake type particle (Fig. 3) morphology. The calcined counterpart shows nearly spherical grains. TEM micrograph of the calcined samples shows particles with sizes between 5 and 25 nm. The TEM/SEM microscopic images also support the powder has porous agglomerates. It is attributed by the fast expulsion of the gases during the combustion. The chemical analysis of the calcined powders as observed by EDS is shown in Fig. 5a and b. The EDS analysis attached with both SEM/TEM confirms the prepared powder has chemical composition as $Ce_{0.9}Sm_{0.1}O_{1.95}$.

The $Ce_{0.9}Sm_{0.1}O_{1.95}$ samples sintered at 1200 °C have theoretical sintered densities as 96.8, 97.0 and 97.6 ± 0.2 for the soaking periods 2, 4 and 6 h, respectively. The sintered densities increase gradually with increasing soaking time. Nearly 98% of theoretical density was obtained for the samples sintered at 1200 °C for 6 h. The SEM micrographs observed on the as-sintered surface of the $Ce_{0.9}Sm_{0.1}O_{1.95}$ pellets showed dense grains. There was no porosity present except the presence of few grain-pull outs. The $Ce_{0.9}Sm_{0.1}O_{1.95}$ samples sintered at 1200 °C for 6 h showed grain size less than 500 nm.

3.2. Electrical characterization

The transport property of the Sm^{3+} doped $Ce_{0.9}Sm_{0.1}O_{1.95}$ samples was analysed by impedance spectroscopy in air. In this work *ac* impedance spectroscopy was used as tool for analyzing the grain

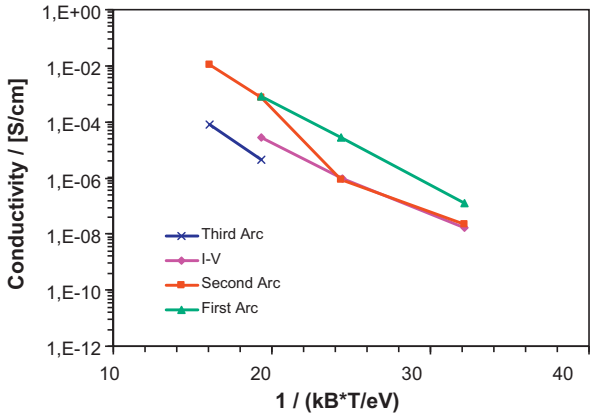

Fig. 7. The Arrhenius plot of the conductivities of grain, grain boundary and the electrode–electrolyte interface behaviour calculated from impedance spectroscopy measurements.

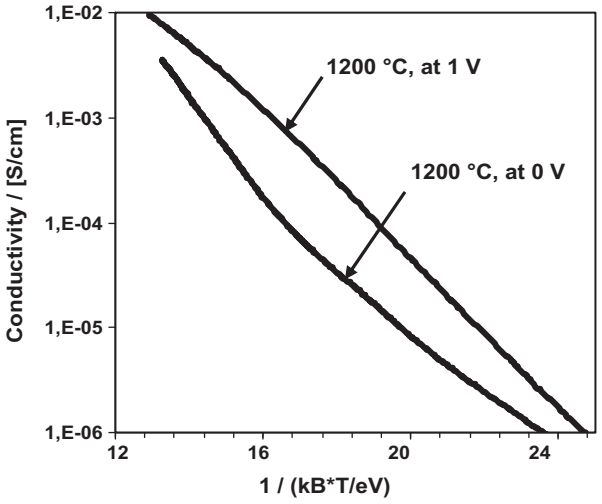

Fig. 8. Thermal activation of conductivity for $Ce_{0.9}Sm_{0.1}O_{1.95}$ sintered at 1200 °C for 6 h.

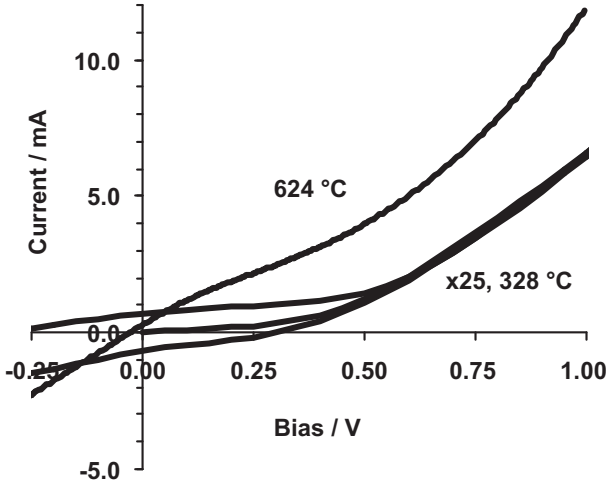

Fig. 9. *dc* current of $Ce_{0.9}Sm_{0.1}O_{1.95}$ sintered at 1200 °C for 6 h (the measurement taken at 328 °C includes a full −5 to +5 V cycle, and is multiplied by 25, for display. The curve taken at 624 °C starts out from −1 V).

and grain boundary conductivity. In a typical *ac* impedance measurement, the complex impedance of the sample as a function of frequency is usually measured. Generally in polycrystalline electroceramics, independent semicircular arcs from high frequency to low frequencies represent the conduction across the grain, grain boundaries and the electrode–specimen interface respectively. As the temperature increases, the arcs shift to higher frequencies, which lead to the successive disappearance of the grain and grain boundary arcs. Finally electrode contribution only will be seen at higher temperatures. Therefore, the grain and grain boundary resistance cannot be separated at high measured temperatures.

In this work the impedance measurements of $Ce_{0.9}Sm_{0.1}O_{1.95}$ sample were conducted at temperatures 88, 203, 328 and 450 °C. The results are shown in Fig. 6(a–d). Fig. 7 shows the Arrhenius plot for these temperatures. Infact, the electrical resistance offered by the sintered $Ce_{0.9}Sm_{0.1}O_{1.95}$ sample was measured and the values were converted to conductivity by the sample dimension. Accordingly the conductivities offered by the grain, grain boundary, and the total were derived at these temperatures. For the temperature ranging between 80 and 450 °C, the impedance plots show three definite arcs that correspond to the grain interior grain boundary and electrode–electrolyte interface (electrode polarization) behaviour.

The electrical conductivity of the sintered $Ce_{0.9}Sm_{0.1}O_{1.95}$ sample with respect to temperature is presented in Fig. 8. It is seen that the conductivity vary linearly within the measured temperatures. In earlier studies the electrical conductivity of ceria was correlated with the dopant type and concentration, sintering temperatures, sintered microstructures, and oxygen partial pressure in the surrounding gas atmosphere [15,16]. In Fig. 8, the procedure consisting 0.5 V bias pulses, around 0 V was used, and the difference in current at the end of 10 s pulses was used to calculate the conductivity. The resulting value may be called difference conductivity around 0 V.

The *I–V* characteristics of the $Ce_{0.9}Sm_{0.1}O_{1.95}$ sample were measured at several temperatures. Representative results, at 328 and 624 °C are shown in Fig. 9. Noting the marked non-linearity of these characteristics, the differential conductivity was calculated, also with 10 s, 0.2 V bias pulses around 1 V and the current difference was taken from the average of the last 3 measurements, at the end of each pulse, i.e. the conductance is calculated as (*I*(1.2 V)–*I*(0.8 V))/0.4 V. This sequence is alternated with the symmetric pulses around −1 V, thus avoiding the possibility of a draft of the results caused by the steady application of bias of a fixed polarity. This procedure leads to the differential conductivity around ±1 V shown in Fig. 9, a region where the current increases quite linearly along with the bias. From the *I–V* curve, the conductivity value was found to be 1×10^{-2} S cm^{-1} at 627 °C. The activation energy in between the temperatures of 100–650 °C was calculated to be 0.84 eV (for phase pure ceria it is reported as 1.03 eV). The electrical conductivity found in this work can be related to pure ionic conductivity (owing to the migration of oxygen ions). Compared to many dopants Sm^{3+} doping produced more stable ceria and this system has least possibility for the reduction of Ce^{4+} to Ce^{3+}, reducible among the rare earth doped ceria materials and moreover we used relatively low temperatures to carry out the electrical conductivity measurements. Low temperatures do not favour the reduction of 4^{+} state of the ceria ion to 3^{+} which is usually responsible for the electron conduction. The activation energy obtained in the present work is well accordance with the previously reported values [17,18] and higher than the value 0.63 eV, reported by Wang et al. [19].

3.3. Thermal properties

Studies on thermal expansion characteristics of doped ceria were widely attempted rather than the thermal conductivity and diffusivity studies. In fact ceria is a preferred top coat in thermal barrier coatings only due to its low thermal conductivity. The thermal conductivity of the sintered oxide ceramics strongly depends on the microstructural features such as surface finish, grain size, and porosity of the sintered material. In an earlier work, Burghartz et al. have reported thermal diffusivity and thermal conductivity of phase pure ceria as 1.96×10^{-6} m^2 s^{-1} and 5.117 W m^{-1} K^{-1}, respectively at 600 K [20]. We have also already reported the thermal conductivity value of Gd-doped CeO_2 [13]. In this work, the room temperature (298.15 K) thermal conductivity and thermal diffusivity properties as studied by photoacoustic technique [12] resulted in the values of 0.5×10^{-6} m^2 s^{-1} and 1.2 W m^{-1} K^{-1}, respectively for the dense $Ce_{0.9}Sm_{0.1}O_{1.95}$ sample sintered at 1200 °C for 6 h. The enhanced densification and fine-grain size are the reasons for high thermal diffusivity and thermal conductivity. The current results of Sm^{3+} doped ceria are in accordance with our earlier work on Gd-doped CeO_2. In nanocrystalline solids, where the grain size is well below a micron, the thermal

conduction is governed by both structural defects as well as grain boundary phonon scattering.

4. Conclusions

Nanocrystalline $Ce_{0.9}Sm_{0.1}O_{1.95}$ was prepared by citrate gel-combustion technique. The nano ceria showed a specific surface area of 50.8 m^2/g in the as-combusted condition that decreased to 36.5 m^2/g after calcination at 700 °C. The nano ceria particles had crystallite size between 6 and 17 nm. Upon sintering the $Ce_{0.9}Sm_{0.1}O_{1.95}$ sample showed 98% theoretical sintered density at sintering temperature of 1200 °C/6 h. The samples had sintered microstructures consisting of dense ceria grains with size less than 500 nm. The electrical conductivity for the combustion derived $Ce_{0.9}Sm_{0.1}O_{1.95}$ samples was found to be of the order of 10^{-2} S cm^{-1} at 600 °C. The apparent activation energy for the oxygen migration was found to be 0.84 eV in the temperature range of 100–650 °C. The photoacoustic technique resulted in room temperature thermal diffusivity and thermal conductivity values of 0.5×10^{-6} m^2 s^{-1} and 1.2 W m^{-1} K^{-1}, respectively for the dense $Ce_{0.9}Sm_{0.1}O_{1.95}$ sample.

Acknowledgements

The authors would like to thank Direction of Investigation, University of Concepción and the FONDECYT funded Projects (Nos. 1100349 and 11080230) by the Government of Chile, Santiago for their financial assistance.

References

[1] V. Esposito, E. Traversa, J. Am. Ceram. Soc. 91 (4) (2008) 1037–1051.
[2] M.-Y. Cheng, D.-H. Hwang, H.-S. Sheu, B.-J. Hwang, J. Power Sources 175 (2008) 137–144.
[3] M. Chen, B.H. Kim, Q. Xu, B.K. Ahn, W.-J. Kang, D.p. Huang, Ceram. Int. 35 (2009) 1335–1343.
[4] L.I. Ji-Guang, T. Ikegami, T. Mori, Acta Mater. 52 (2004) 2221–2228.
[5] M.R. Kosinski, R.T. Baker, J. Power Sources 196 (2011) 2498–2512.
[6] Y. Liu, w.B. Li, X. Wei, W. Pan, J. Am. Ceram. Soc. 91 (12) (2008) 3926–3930.
[7] C. Peng, Y. Wang, K. Jiang, B.Q. Bin, H.W. Liang, J. Feng, J. Meng, J. Alloys Compd. 349 (2003) 273–278.
[8] D.A. Andersson, S.I. Simak, N.V. Skorodumova, I.A. Abrikosov, B. Johansson, Proc. Natl. Acad. Sci. 103 (10) (2006) 3518–3521.
[9] C. Wan, W. Pan, Z. Qu, Y. Qin, Key Eng. Mater. 336–338 (2007) 1773–1775.
[10] R.V. Mangalaraja, J. Mouzon, P. Hedström, I. Kero, K.V.S. Ramam, C.P. Camurri, M. Odén, J. Mater. Process. Technol. 208 (1–3) (2008) 415–422.
[11] B.D. Cullity, Elements of X-ray Diffraction, Second edition, Addison-Wesley, MA, 1978.
[12] K. Raveendranath, J. Ravi, R.M. Tomy, S. Jayalekshmi, R.V. Mangalaraja, S.T. Lee, Appl. Phys. A 90 (2008) 437–440.
[13] R.V. Mangalaraja, S. Ananthakumar, M. Paulraj, M. López, C.P. Camurri, R.E. Avila, Process. Appl. Ceram. 3 (3) (2009) 137–143.
[14] J. Leitner, P. Chuchvalec, D. Sedmidubsky, A. Strejc, P. Abrman, Thermochim. Acta 395 (2003) 27–46.
[15] S. Hui, J. Roller, S. Yick, X. Zhang, C.D. Petit, Y. Xie, R. Maric, D. Ghosh, J. Power Sources 172 (2007) 493–502.
[16] H. Inaba, H. Tagawa, Solid State Ionics 83 (1996) 1–16.
[17] W. Huang, P. Shuk, M. Greenblatt, Chem. Mater. 9 (1997) 2240–2245.
[18] R.T. Dirstine, R.N. Bluementhal, T.F. Kuech, J. Electrochem. Soc. 126 (2) (1979) 264–269.
[19] Y. Wang, T. Mori, J.-G. Li, Y. Yajima, Sci. Tech. Adv. Mater. 4 (2003) 229–238.
[20] M. Burghartz, Hj. Matzke, C. Léger, G. Vambenepe, M. Rome, J. Alloys Compd. 271–273 (1998) 544–548.